Summer Climate Change in the Midwest and Great Plains due to Agricultural Development during the Twentieth Century

CATHERINE A. NIKIEL AND ELFATIH A. B. ELTAHIR

Parsons Laboratory, Massachusetts Institute of Technology, Cambridge, Massachusetts

(Manuscript received 4 February 2019, in final form 6 June 2019)

ABSTRACT

Agricultural development is among the most significant forms of land-use change globally. In central North America it has consisted of cropland expansion in the early 1900s, yield intensification starting in the 1930s, and the development of large irrigated areas beginning in the 1950s. The area of this study encompasses the Midwest and Great Plains of the United States not only because significant agricultural change has occurred here but also because of the significant cooling (warming hole) there in the midcentury. This study investigates the relative contribution of agricultural development and greenhouse gas (GHG) emissions on the observed patterns of regional changes in summer temperature, precipitation, and evapotranspiration using a long-term twentieth-century reanalysis dataset (CERA-20C) as boundary conditions for simulations with the MIT Regional Climate Model (MRCM). Temperatures in the Great Plains (33°–43°N, 95°–109°W) and the Midwest (38°–48°N, 82°–109°W) would have been significantly higher in the second half of the twentieth century without the influence of agricultural development, largely due to an increase in evaporative cooling. The simulations of precipitation changes reflect a significant influence of global SST teleconnections at decadal time scales. Numerical simulations also demonstrate the competing effects of cropland expansion and yield intensification on shaping the observed pattern of increases in precipitation. Ultimately, a combination of agricultural development and decadal variability of global sea surface temperatures (SST) explains most of the observed variability of summer temperature and precipitation during the twentieth century over central North America.

1. Introduction

The Midwest and Great Plains of the United States contain some of the most productive and expansive areas of agricultural land in the country as well as sizable proportions of the population. This area, colloquially known as the Cornbelt, is one of the highest yielding global agricultural areas for maize (Ben-Ari and Makowski 2014) and the United States is a leading exporter of soybeans and corn (Simoes 2016a,b). Additionally, urban centers such as Chicago, Illinois; Indianapolis, Indiana; and Columbus, Ohio are in the top 20 most populous cities in the United States (U.S. Census Bureau 2017).

While definitions of the Midwest and Great Plains differ, this study focuses on states that encompass the areas of highest agricultural development and production—North Dakota, South Dakota, Nebraska, Kansas, Minnesota, Wisconsin, Missouri, Michigan, Iowa, Illinois, Indiana, and Ohio. Agricultural development has dominated land use change in this region during the twentieth century and is an increasingly important area of focus for climate studies (Pielke et al. 2011, 2016). Cropland areas are particularly sensitive to drought and other extreme conditions, and the economic importance of this region makes understanding regional and local climate impacts here a particular concern. Assessments have noted that damages to agriculture in these regions from drought, floods, and extreme heat are among the biggest threats in a changing climate (USGCRP 2018).

While crops are impacted by climate change, large-scale agricultural land use has been shown to have climate feedbacks. Several studies suggest that rapidly changing land use conditions in the twentieth century may have partially masked the signal of greenhouse gas (GHG)-triggered climate change in this region (Bonfils and Lobell 2007; Kueppers et al. 2007). Therefore, it is reasonable to ask not only how crops will fare in different climate conditions, but also how crops and agricultural

Supplemental information related to this paper is available at the Journals Online website: https://doi.org/10.1175/JCLI-D-19-0096.s1.

Corresponding author: Catherine A. Nikiel, nikiel@mit.edu

DOI: 10.1175/JCLI-D-19-0096.1

development can impact the climate in the long term. As patterns of agricultural expansion and intensification change in the future, the balance between greenhouse gas–induced atmospheric changes and land use impacts will shift, and the trends of previous decades may not be applicable to future projections.

Cropland expansion and redistribution has been widespread in the central United States in the nineteenth and twentieth centuries. Cropland areas have largely disappeared in the East while they have replaced open grassland in the Great Plains up through Canada. Small fluctuations occurred throughout the twentieth century but the majority of changes in cropland distribution happened prior to the 1940s (see Fig. S1a in the online supplemental material).

Another major agricultural change has been an increase in yield. Corn has seen an average yield increase, weighted by state production, in the Midwest of 370% from 1900 to 2016, with almost all the increase occurring after 1935 (USDA-NASS 2016) (Fig. S1b). Soybean has seen a weighted average yield increase of 400% from 1924 to 2016 (Fig. S1c). While the larger trends in both of these crops are positive and linear, the time series are marked by a large interannual yield variability, and clearly show losses attributed to major seasonal events such as drought in 1988 and floods in 1993 (Figs. S1b,c) (Ben-Ari and Makowski 2014).

Another component of agricultural evolution in the United States is the expansion of irrigation, which started intensively at around the same time that crop yields began to increase (Siebert et al. 2015). While the focus is mostly on agricultural development and climate change within the central United States, there are several other important irrigation areas in the Texas Panhandle and the Mississippi River valley that are included within the model domain. Irrigation most directly affects soil moisture at the site of application and, through this, the hydrologic cycle. Evapotranspiration and latent heat flux, a measure of the turbulent transport of moisture away from the surface and into the atmosphere, are increased over irrigated areas (Eltahir 1998; Adegoke et al. 2003; Ozdogan et al. 2010; Harding and Snyder 2012; Lo and Famiglietti 2013; Qian et al. 2013; Huber et al. 2014; Cook et al. 2015). Sensible heat flux, the complementary component of turbulent heat transfer away from the surface, is reduced as a result. This increase in latent heat flux is accompanied by surface cooling in irrigated areas (Kueppers et al. 2007; Huber et al. 2014; Qian et al. 2013; Mueller et al. 2015; Jin and Miller 2011; Lobell et al. 2008). Similar cooling effects have been shown over agricultural areas in the Midwest due to agricultural intensification (Mueller et al. 2015; Alter et al. 2018).

Additionally, it has been proposed that irrigation increases precipitation downwind of the irrigated area, to a greater degree and even in the absence of precipitation over the area itself (DeAngelis et al. 2010; Lo and Famiglietti 2013; Huber et al. 2014; Im and Eltahir 2014; Im et al. 2014; Alter et al. 2015a,b; Lu et al. 2017). These effects are tied to an alteration of the large-scale circulation, atmospheric moisture content, and convective environment (Pal and Eltahir 2002; Kueppers et al. 2007; Im et al. 2014; Alter et al. 2015a,b; Cook et al. 2015; Halder et al. 2016; Lu et al. 2017). Correspondingly, decreases in planetary boundary layer (PBL) height have been found due to modification of energy and moisture fluxes, although studies note that there is uncertainty regarding the ultimate impact on convective potential directly over irrigated areas due to competing effects (Jin and Miller 2011; Harding and Snyder 2012; Qian et al. 2013; Im and Eltahir 2014; Im et al. 2014; Lu et al. 2017). Additionally, several studies have noted that circulations induced by cooling over irrigated areas can either augment or counter existing atmospheric patterns such as the low-level jet (LLJ) (Huber et al. 2014) or monsoonal circulation (Im et al. 2014) and influence the overall pattern of moisture advection and precipitation.

A study of the effects of agricultural development in this region of the United States is justified due to the anomalous observed changes in summer temperature and precipitation that have occurred in this area in the latter half of the twentieth century, dubbed the *warming hole*. Although the position, intensity, and proposed causes of the warming hole differ depending on the framing of the study, multiple recent studies have shown the presence of a summer warming hole (Fig. 1) located in the central United States and have proposed agricultural land use change as a cause (Pan et al. 2017; Partridge et al. 2018; Mascioli et al. 2017; Alter et al. 2018). For example, Douglas (2016) identified a "region of significant change" (ROSC) (39°–48°N, 100°–82°W) and showed that a comparison of 1920–49 to 1970–99 climatologies highlighted a period of significant change, corresponding with both irrigation expansion and productivity growth. Observed changes in temperature (Mueller et al. 2015), precipitation (Alter et al. 2018), and humidity (Brown and DeGaetano 2013) in this region have been attributed to agricultural land use changes. The U.S. warming hole is a rare, but not unique, phenomenon. Central and eastern China have also experienced a similar cooling and wetting over the same period (see Alter et al. 2018; see also Figs. S3 and S4 in the online supplemental material) and Zhang et al. (2016) identified a late-century warming hole through an analysis of summer maximum and minimum temperature ratios.

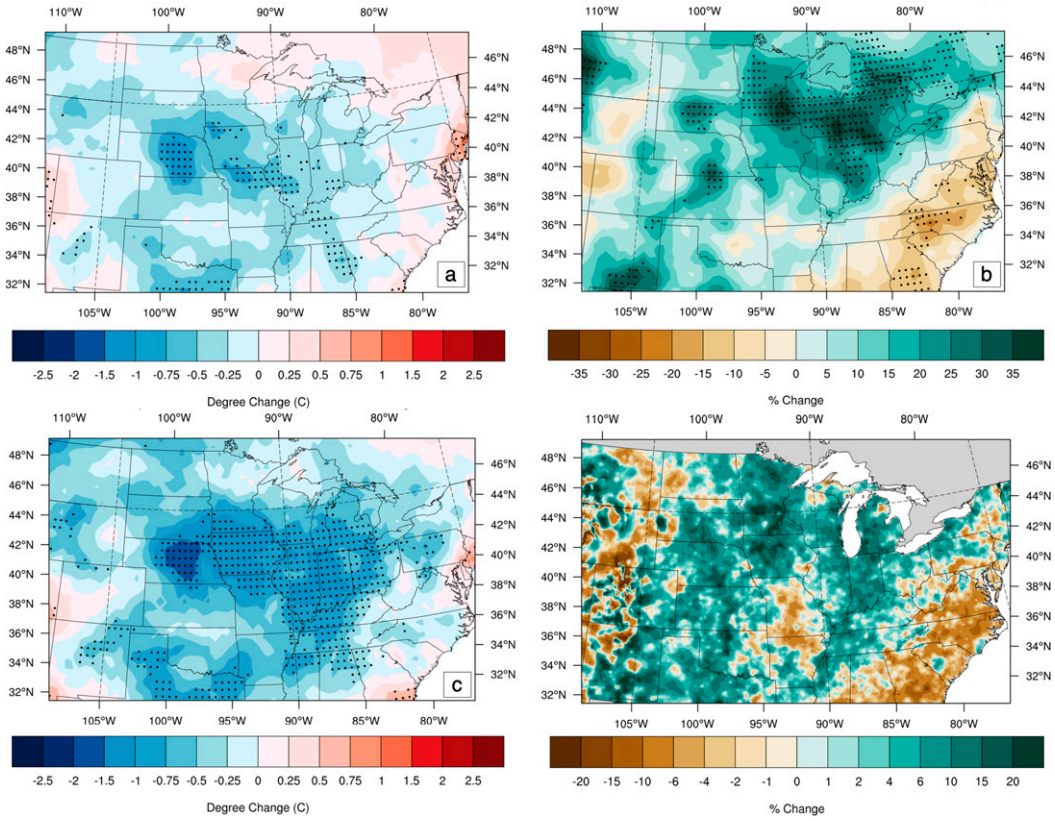

FIG. 1. Observed changes in (a) mean surface temperature (CRUTS4.01), (b) precipitation (CRUTS4.01), (c) maximum surface temperature (CRUTS4.02), and (d) evapotranspiration (Livneh et al. 2013). Change shown is the difference between July–August monthly average from 1920–49 to 1970–99. Stippling shows a significant change between the two periods according to a Kolmogorov–Smirnov test at the 5% significance level.

Natural internal variability can also influence regional climate on decadal and centennial scales. Sea surface temperature has been a well-documented forcing of seasonal precipitation and temperature changes in the United States (USGCRP 2018). In general, drought conditions and warmer summertime temperatures in central North America are connected to a cold Pacific Ocean and a warm Atlantic Ocean (Ting and Wang 1997; Schubert et al. 2004; Seager et al. 2008; Schubert et al. 2009; Wang et al. 2009; Findell and Delworth 2010; Ruiz-Barradas and Nigam 2010; Wang et al. 2010; Cook et al. 2011; Seager and Hoerling 2014; Wang and Schubert 2014; Donat et al. 2016; Jia et al. 2016), with many studies emphasizing the role of either the Pacific (Schubert et al. 2004; Alfaro et al. 2006; Koster et al. 2009; Schubert et al. 2009; Findell and Delworth 2010; Wang et al. 2010; Mei and Wang 2011; Burgman and Jang 2015; Jia et al. 2016) or the Atlantic (Enfield et al. 2001; Knight et al. 2006; Kunkel et al. 2006; Weaver and Nigam 2008; Weaver et al. 2009; Nigam et al. 2011). In particular, the correlation to the North Atlantic is strong for the analysis regions in this study (Table 1). Figure S2 in the supplemental material shows the Pearson correlation coefficient between grid cell time series of July–August averaged precipitation and the area averaged North Atlantic SST in the same months. The observed changes in precipitation in the CRU data are also shown for comparison. The pattern of correlation closely matches the observed changes and are consistent with the changes that might be expected as the North Atlantic transitioned from a very warm period in 1920–49 to a very cool period in 1970–99 (Fig. S3).

2. Data

The experiments conducted in this study are made possible through the use of several newly developed datasets, allowing for a more in-depth picture of the changes that have occurred in this region over the course of the entire twentieth century. The reanalysis dataset used here to provide lateral boundaries and initial conditions for the historical runs is CERA-20C, developed by the European Centre for Medium-Range Weather Forecasts (ECMWF) (ECMWF 2017). CERA-20C is

TABLE 1. Pearson correlation coefficients between July–August area-averaged, standardized, detrended anomalies of CRU temperature and precipitation and the following SST time series. One asterisk (*) indicates significance at $p = 0.05$ and two asterisks (**) indicate significance at $p = 0.01$.

	Midwest temperature	Great Plains temperature	Midwest precipitation	Great Plains precipitation
North Atlantic (Donat et al. 2016)	0.31**	0.34**	−0.43**	−0.20*
Tropical Pacific (Mei and Wang 2011)	−0.20*	−0.18	0.29**	0.24**
Central North Pacific (Mei and Wang 2011)	0.25**	0.16	−0.25**	−0.15

the newest generation product developed through the ERA-CLIM2 project developed on 91 atmospheric model levels and with a land resolution of 125 km with four soil layers and an ocean grid resolution of 110 km with 42 levels (ECMWF 2017). This coupled ocean–atmosphere product assimilates sea surface pressure from the International Surface Pressure Databank (ISPD) and the International Comprehensive Ocean–Atmosphere Dataset (ICOADS) as well as marine winds from ICOADS; CERA-20C also uses ocean temperature and salinity profiles from HadISST2 (Laloyaux 2017). The simulations are run with ensemble member 5 from the 10-member product. This ensemble member was chosen because it exhibits less of a warm bias in the early centuries than the other members in the region of interest.

However, caution must be used in interpretation of early-century simulations as there is evidence that the reanalysis data are less reliable. There is a wide spread in the 10-member ensemble of CERA-20C, although this stabilizes in the midcentury (Figs. 2a,b). More evidence for reanalysis shortcomings is seen in an intense cooling feature in Canada that does not exist in the observations (Figs. 2c–e). This anomalous cooling is present in CERA-20C and another ECMWF product, ERA-20C (Poli et al. 2016), as well as in NOAA 20CR V2c developed by the National Oceanic and Atmospheric Administration (NOAA) in collaboration with the Cooperative Institute for Research in Environmental Sciences (CIRES) (Compo et al. 2011). The analysis methodology was chosen with these potential problems in mind, and an attempt was made to minimize their

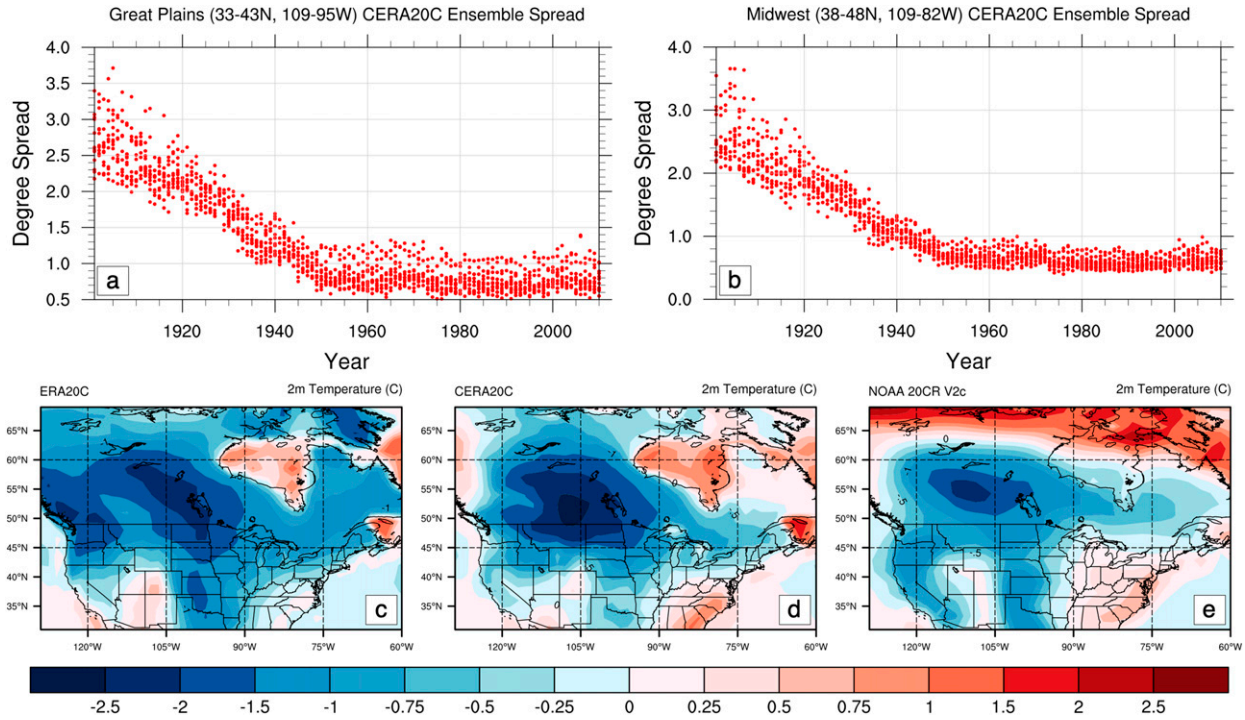

FIG. 2. (a) CERA-20C ensemble spread in temperatures (K) averaged over the Great Plains. (b) As in (a), but for the Midwest. (c) July–August average temperature change (°C) from 1920–49 to 1970–99 in ERA-20C 2-m temperature (ECMWF). (d) As in (c), but for CERA-20C. (e) As in (c), but for NOAA 20CR V2c.

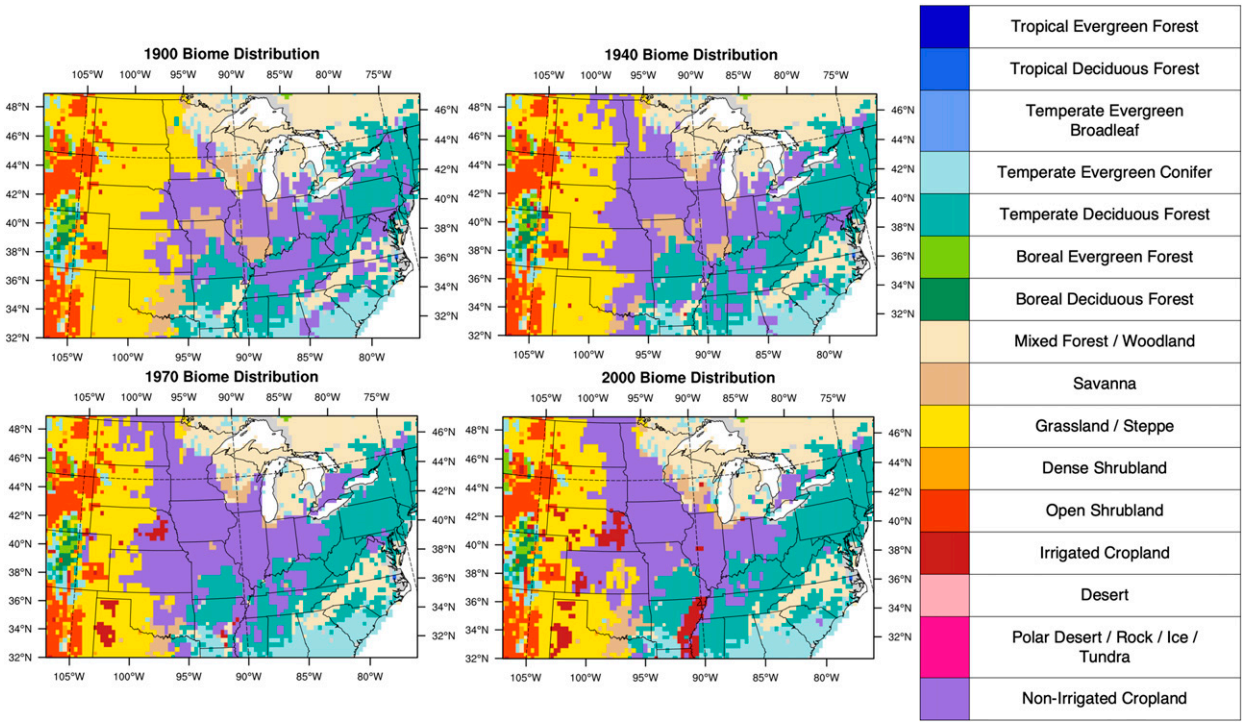

FIG. 3. Biome distribution maps used as land surface input to IBIS for select years.

impacts on the results. Although anomalous boundary condition features will appear in results that present a single simulation, results that show the changes dues to vegetation and GHG are free of boundary condition error because all simulations are conducted with the same set of boundary conditions. This cooling feature provides further justification for the use of ensemble 5, as the cooling is less intense and widespread than in some of the other members.

Land surface boundary conditions are compiled from three separate data sources: 1) a 5-min resolution potential vegetation dataset (Ramankutty and Foley 1999), 2) the Harmonized Global Land Use Dataset 1500–2100 (LUHv1) for cropland designation at 0.5° resolution (Hurtt et al. 2011; Chini et al. 2014), and 3) the Historic Irrigation Dataset (HID) at 5-min resolution (Siebert et al. 2015). A composite land surface dataset was then developed for each decade (Fig. 3). If a grid cell is occupied by at least 50% cropland, then the entire grid cell is designated as the nonirrigated cropland biome. If a grid cell contains at least 25% irrigation, the grid cell is designated as the irrigated cropland biome. These thresholds were selected to ensure that the largest areas of development are present in the land use map while not overestimating agricultural area in other regions. While this omits areas of diffuse irrigation it captures the large-scale development that occurred in the Texas Panhandle, Kansas, eastern Nebraska, and the lower Mississippi River valley.

To determine agricultural intensification, data on acres harvested, acres planted, and yield for corn were obtained from the U.S. Department of Agriculture's (USDA) National Agricultural Statistics Service (NASS) (USDA-NASS 2016). Yield can be translated to net primary production (NPP) through an inventory-based method that has been used widely (Prince et al. 2001; Hicke and Lobell 2004; West et al. 2010; Monfreda et al. 2008; Bandaru et al. 2013; Li et al. 2014; Jaafar and Ahmad 2015). This yield increase was then designated within the model by a modification of the net crop photosynthesis rate, as net primary production is a measure of the amount of carbon fixed into new biomass in vegetation and can broadly be described as the difference between photosynthetic production and respiration (Roxburgh et al. 2005). NPP rates in the model were tuned to a corn equivalent NPP derived from a reconstructed 1992 NPP spatial map developed by Prince et al. (2001). In the model cropland has the physiological characteristics of a C_4 pathway crop and therefore all values were determined as corn NPP equivalent for consistency.

Observed temperature and precipitation data come from the Climatic Research Unit Time Series (CRUTS4.01) developed by the University of East Anglia, which spans

1901–2016 at 0.5°(latitude) × 0.5°(longitude) resolution (Harris et al. 2014). Historical trends in evapotranspiration data are taken from the Livneh daily CONUS near-surface gridded meteorological and derived hydrometeorological data provided by the NOAA/OAR/ESRL PSD, Boulder, Colorado, from their website at https://www.esrl.noaa.gov/psd/, which are available from January 1915 to December 2011 at 1/16°(latitude) × 1/16°(longitude) resolution (Livneh et al. 2013). SST observations are taken from the Extended Reconstructed Sea Surface Temperatures Version 5 (ERSSTv5) (Huang et al. 2017). In this study, the SST regions used are the North Atlantic [37°–53°N, 303°–317°E, closely matching Donat et al. (2016)], tropical Pacific (1°S–9°N, 197°–209°E), and central North Pacific (29°–35°N, 179°–195°E) where the latter two are roughly derived from regions used in Mei and Wang (2011).

The ocean boundary conditions are set using the Hadley Centre Sea Ice and Sea Surface Temperature dataset (HadISSTv1.1) provided by the Met Office Hadley Centre in collaboration with the National Oceanography Centre, Southampton, and the Lamont-Doherty Earth Observatory of Columbia University (Rayner et al. 2003). Finally, GHG concentrations were designated annually for CO_2, CH_4, N_2O, CFC-11, and CFC-12 using the concentrations approved for use in the CMIP5 project and in preparation for the Intergovernmental Panel on Climate Change (IPCC) Fifth Assessment Report (Meinshausen et al. 2011).

3. Methodology

The simulations for this study were performed using the MIT Regional Climate Model (MRCM). MRCM is an updated version of the Regional Climate Model version 3 (RegCM3) climate model, originally developed at the National Center for Atmospheric Research (NCAR) and maintained by the International Center for Theoretical Physics (ICTP). The model has been further modified by the Eltahir research group to improve representations of albedo, dust emissions, cloud and convection schemes, and boundary layer dynamics (Marcella and Eltahir 2010, 2012; Gianotti et al. 2012; Gianotti and Eltahir 2014a,b). MRCM is composed of an atmospheric circulation model coupled with a land surface model. The present setup uses the Grell Cumulus Scheme with the Arakawa and Schubert convective closure assumption (Arakawa and Schubert 1974; Grell 1993). This combination has been shown as the most appropriate in previous studies of the midwestern United States (Winter 2006; Winter and Eltahir 2012a,b). A vital development for MRCM was the replacement of the original land surface model, the Biosphere–Atmosphere Transfer Scheme (BATS), with the Integrated Biosphere Simulator (IBIS) (Winter 2006). Several studies have noted the suitability of RegCM3 (Diffenbaugh et al. 2005; Kueppers et al. 2007; Diffenbaugh 2009), and of a coupled RegCM3-IBIS framework, for regional climate modeling in the central United States (Winter and Eltahir 2012a,b).

TABLE 2. Description of simulation experiments.

	Boundary conditions	GHG	Vegetation
nV-nG	Evolving	Static	Static
nV-G	Evolving	Evolving (annual)	Static
V-G	Evolving	Evolving (annual)	Evolving (decadal)

A three-member ensemble per experiment set of simulations is presented here. All simulations are run on a domain centered at 40.5°N, 91.5°W with a 30-km grid spacing, and 122 zonal points, 80 meridional points, and 18 vertical sigma levels. The outer nine grid cells are not included in analysis in order to avoid any boundary effects. The CERA-20C simulations are run from 1 January, 2 January, or 3 January 1901 depending on the ensemble through 31 December 2005. Each set is composed of three simulations: 1) no vegetation development and no GHG increases (nV-nG), 2) no vegetation development with realistic GHG increases (nV-G), and 3) vegetation development and realistic GHG increases (V-G) (Table 2).

The simulations with no vegetation development and no GHG were run with 1900 conditions for those parameters respectively. The V-G simulation in each of the sets is run in decadal segments (except the first simulation, which is run from 1901 to 1905), with the land use map being updated to reflect cropland and irrigation expansion in the 10 years surrounding 1900, 1910, 1920, etc. The decadal runs were run with one extra year at the beginning of each of the decadal simulations (starting 1–3 January depending on the ensemble), which was not used in the postprocessing and the construction of the full time series.

Soil moisture conditions are equilibrated for the region with long-term offline simulations of IBIS, and no longer spinup time was needed to establish equilibrium. Irrigation was initially introduced into MRCM for testing land–atmosphere processes in semiarid regions, and the original irrigation scheme was set to return the root zone soil moisture at every time step to the weighted average root zone field capacity in each of the four top layers that make up the root zone (0–100 cm) (Marcella 2013). The same irrigation setup was later used to investigate the effects on precipitation in the Gezira

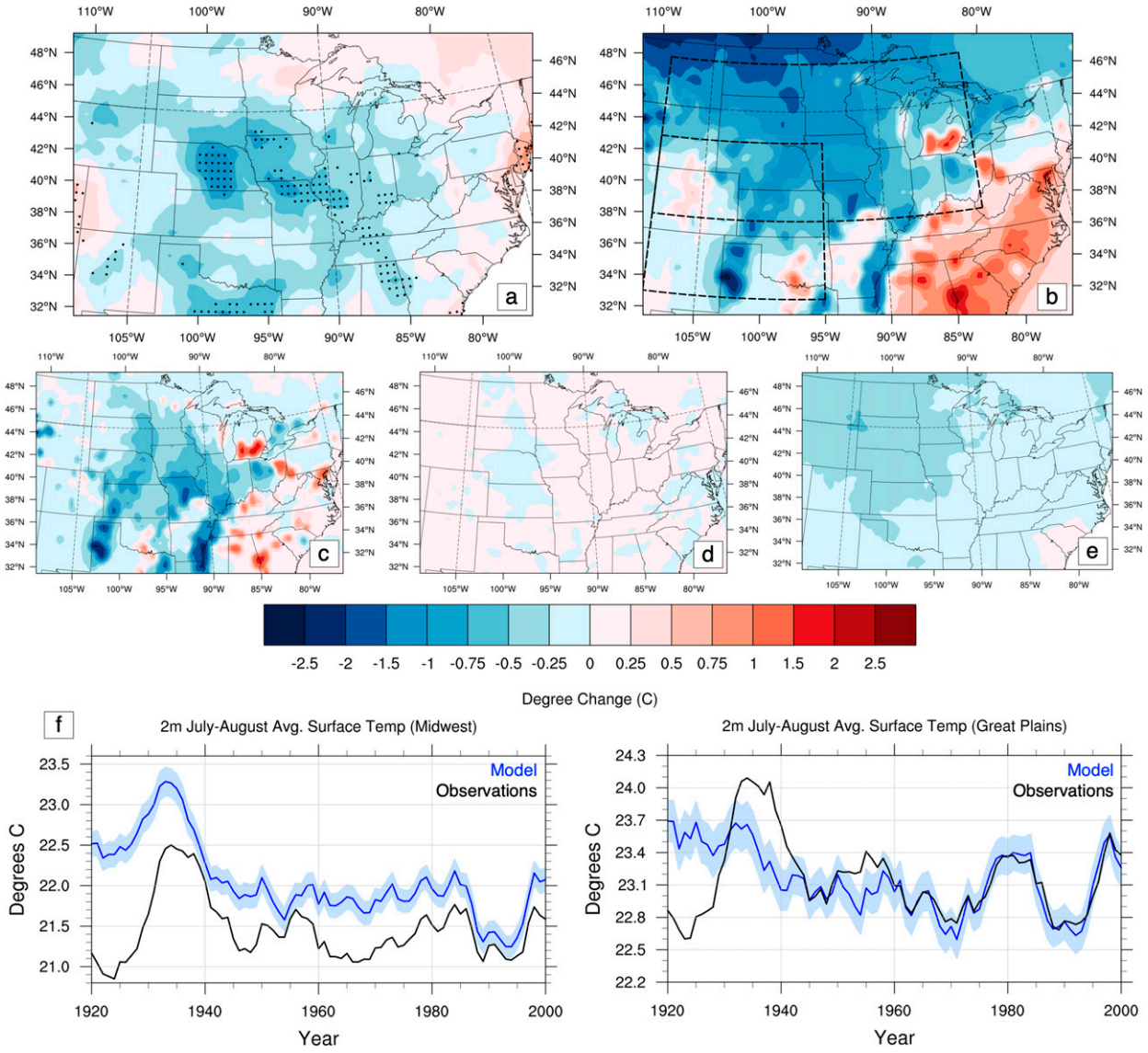

FIG. 4. (a) July–August mean surface temperature change (°C) from 1920–49 to 1970–99 in observation (CRUTS4.01) data, (b) change in V-G simulation, (c) change due to vegetation in simulations, (d) change due to GHG in simulations, and (e) estimates of temperature change attributed to SST in the North Atlantic (37°–53°N, 303°–317°E), tropical Pacific (1°S–9°N, 197°–209°E), and central North Pacific (29°–35°N, 179°–195°E) using a multilinear regression to observed CRU temperature. (f) Time series of area-averaged temperature in the model ensemble (blue) with shading representing the standard deviation of the three-run ensemble. CRU data are shown in black.

region in East Africa and in West Africa in conjunction with the West African monsoon (Im and Eltahir 2014; Im et al. 2014; Alter et al. 2015b). In the current setup, the model is slightly modified in order to more realistically represent irrigation in the region. Rather than replenishing the root zone constantly, irrigation is applied when a threshold of 75% of average root zone relative field capacity is reached. Additionally, irrigation is restricted from July to September rather than May to September, which aligns with a restriction on crop growth before July.

The analysis is performed for two main regions, the Great Plains (33°–43°N, 95°–109°W) and the Midwest (38°–48°N, 82°–109°W). The ROSC identified by Douglas (2016) is mostly included within these two regions, but the distinction is made between these two analysis regions in order to be mindful of differences in seasonal precipitation climatology, SST teleconnection influences, and differing components of agricultural development. The time periods of comparison are 1920–49 (early period) and 1970–99 (late period), which are consistent with Douglas (2016) and Alter et al. (2018).

Additionally, all averages are shown for July–August. This time period is chosen to capture the time period of maximum vegetative growth and irrigation impacts and to allow for comparison to previous studies (Adegoke et al. 2003; Ozdogan et al. 2010; DeAngelis et al. 2010; Alter et al. 2018). Where appropriate, area averaged changes are accompanied by description of significance from the results of Kolmogorov–Smirnov two sample test (K-S test) at a 95% confidence level ($N = 30$) (Heckert and Filliben 2003; Sheskin 2007).

4. Results and comparison to observations

a. Temperature

In the observational data, temperatures cooled an average of 0.31°C (0.16°C) in the Great Plains (Midwest) between the early and late period, with isolated cooling in the Midwest of 1°–1.5°C (Fig. 4a). These areas of cooling are surrounded by warming along the East Coast and into the Northeast and Canada, as well as in the West.

While differences exist in the spatial distribution of temperature changes and the magnitude of peak cooling and warming, cooling occurs in both observations and simulations through the central Great Plains and Midwest. Overall, agricultural development led to widespread cooling throughout the domain, particularly in areas that are irrigated or intensified over the simulation period (Fig. 4c). Pockets of heating are seen in the East, due to the reduction of cropland in the land use dataset, and the reversion to forest type biomes present in the potential vegetation dataset. Whether this reforestation actually occurred is beyond the scope of this study and is a limitation of the development of the land use dataset. GHGs lead to overall warming in the domain with patches of cooling (Fig. 4d). The magnitude of this change is much smaller than the change due to the vegetation or the background conditions. To estimate the impact of SST, a multilinear regression was conducted at every grid point between the three SST regions identified earlier and CRU observational data. The time series were detrended as before. The SST impact on temperature is shown to be weaker than vegetation, and also concentrated in the northwest of the domain, not aligned with the major agricultural areas, and offset from the observed pattern of change (Fig. 4e). Impacts of the individual SST regions calculated using linear regression can be seen in Fig. S4, and it can be seen that the North Atlantic contributes most to the modeled change.

The largest deviations in the cooling pattern are due to the influence of the boundary conditions and associated errors (Fig. S5). The abnormal cooling in the Northwest of the domain and heating along the East Coast in this component has a strong influence on the overall change, compared to the impact of vegetation and GHG in these areas. The simulations have more skill in matching the observed temperatures in the two regions after 1950, especially in the Great Plains (Fig. 4f), and this again points to the increased reliability of boundary conditions post-1950.

TABLE 3. Modeled temperature changes (°C) due to vegetation (Veg) and GHG in the model simulations. The final row shows these modeled effects removed from the observed (Obs) changes in the CRU dataset to provide an estimate of change due to natural variability and other natural or anthropogenic forcings.

	Great Plains	Midwest
Vegetation impact	−0.32	−0.24
GHG impact	0.02	0.02
Natural variability (Obs − GHG − Veg)	0.01	−0.06

Table 3 shows the area averaged changes in temperature attributed to agricultural development (expansion of cropland, development of irrigation, and intensification) and GHG. The vegetation impact is shown to have an order of magnitude more impact than GHG on these regions. The temperature effect due to vegetation is higher in the Great Plains likely due to the enhanced cooling in irrigated areas. Averaging over grid cells that are designated as nonirrigated (irrigated) cropland in the 2000 land use map, the average temperature change associated with the agricultural development is a cooling of 0.6°C (1.5°C). The average irrigated cooling compares well to the July irrigation mean cooling of 1.4°C in Adegoke et al. (2003), while Lobell et al. (2009) found an irrigation cooling of 0°–10°C with 5°C or more in the dry season. Alter et al. (2018) found a cooling of 1°C in intensified cropland areas. The average cooling from vegetation and heating from GHG in these regions was able to collectively approximate the observed cooling.

The ''residual'' change in these regions is found to be small, and on the order of the impact from GHG between the early and late periods. This suggests that the bulk of the surface cooling in mean July–August temperatures between these two periods in these regions can be attributed to agricultural development, and that natural variability likely played a minimal role in creating the spatial pattern of the temperature change between these two periods.

b. Precipitation

In the observational data, precipitation increased an average of 0.18 mm day^{-1} (0.34 mm day^{-1}) in the Great Plains (Midwest) between the early and late period, which amounts to an increase of 9% (16%), with isolated increases in the Midwest of 30% (Fig. 5a). The

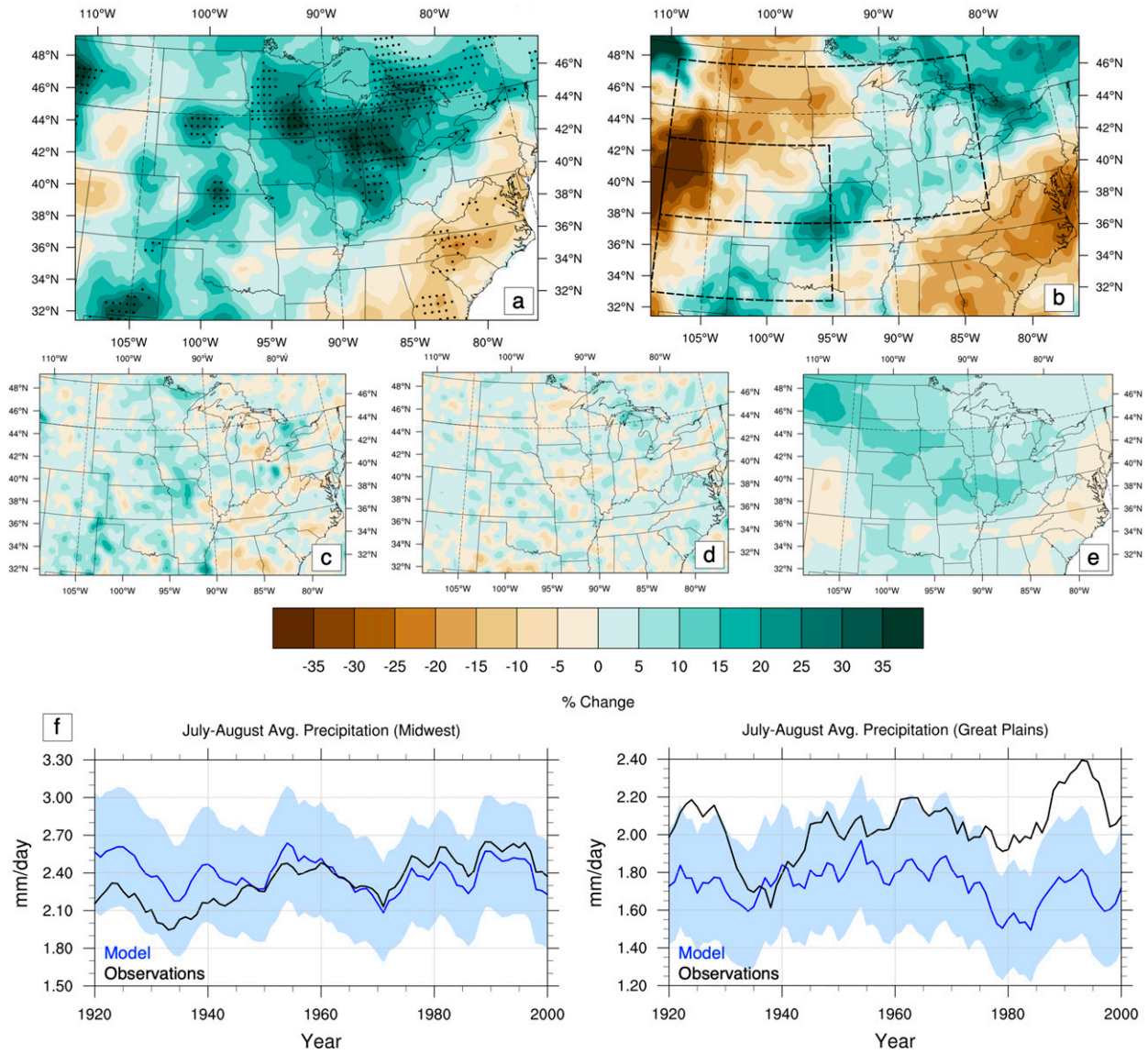

FIG. 5. (a) July–August mean precipitation change (%) from 1920–49 to 1970–99 in observation (CRUTS4.01) data, (b) change in V-G simulation, (c) change due to vegetation in simulations, (d) change due to GHG in simulations, and (e) estimates of precipitation change attributed to SST in the North Atlantic (37°–53°N, 303°–317°E), tropical Pacific (1°S–9°N, 197°–209°E), and central North Pacific (29°–35°N, 179°–195°E) using a multilinear regression to observed CRU precipitation. (f) Time series of area averaged precipitation in the model ensemble (blue) with shading representing the standard deviation of the three-run ensemble. CRU data are shown in black.

increase in precipitation that occurs in the central United States contrasts with the drying that occurs to the east of the Appalachian Mountains.

A dominant pattern of precipitation changes—a dry–wet–dry banding moving from the northwest to the southeast—is captured in the simulations as well as the observations (Figs. 5a,b). However, the strongest precipitation feature in the observations—wetting in Great Plains and particularly in the Midwest—is not present as a distinct feature in the simulations, although both show an average increase in precipitation in this area. The increases in precipitation due to vegetation resemble the pattern of increase seen in the observations (Fig. 5c).

GHG do not cause a distinct pattern of precipitation change (Fig. 5d) and the precipitation increases caused by vegetation are similar in spatial pattern but do not match the intensity of observed change. While changes broadly occur in areas of agriculture development there does not seem to be a distinct pattern of change associated with irrigation specifically. There is an increase in precipitation of 4.3% and 5.2% in nonirrigated and

TABLE 4. Modeled precipitation changes (mm day^{-1}) due to vegetation (Veg) and GHG in the model simulations. The final row shows these modeled effects removed from the observed (Obs) changes in the CRU dataset to provide an estimate of change due to natural variability and other natural or anthropogenic forcings.

	Great Plains	Midwest
Vegetation impact	0.08	0.06
GHG impact	0.03	0.03
Natural variability (Obs − GHG − Veg)	0.09	0.25

irrigated areas respectively. Alter et al. (2018) found an increase in July–August rainfall of 0.15–0.45 mm day^{-1} (5%–15%) due to intensification over large areas the Great Plains with isolated increases of 0.6 mm day^{-1} (20%). Lo and Famiglietti (2013) found an increase in summer rainfall of 15% in their study of irrigation impacts in the California Central Valley. The decrease in precipitation percentage in the West is attributed to the residual forcing (Fig. S6), although the strong magnitude is likely due to a decrease in an already dry area.

Precipitation change due to vegetation changes in the simulations is roughly double the impact from GHG (Table 4). However, unlike in the temperature results, the ''residual'' change in these regions is not negligible, especially in the Midwest where nearly 75% of the observed change is not explained by either vegetation or GHG increases in the model simulations. This suggests that one or more additional forcings contributed to the July–August average precipitation changes over this area between the early and late period. However, the patterns of precipitation change in the full simulations were shown to resemble the observed change. Therefore, it is reasonable to explore the influence of natural variability on this pattern. This variability in the form of SST-forced precipitation change estimates was calculated in the same way as for temperature, and the result is an increase centered in the area of agricultural change, with corresponding drying in the East (Fig. 5e). The coherency and strength of the estimated change attributed to SST is greater than the simulation-based impacts of vegetation and GHGs. Impacts of the individual SST regions calculated using linear regression can be seen in Fig. S4, and it can be seen that the North Atlantic contributes most to the modeled change.

c. *Evapotranspiration*

Evapotranspiration does not have a long-term observational analog. However, comparisons to independent reconstructions of evapotranspiration change in the region show that the spatial pattern of vegetation-induced evapotranspiration changes in MRCM simulations closely matches the pattern in the independent dataset developed using the variable infiltration capacity (VIC) model (Livneh et al. 2013). Increases in evapotranspiration occur throughout much of the agricultural area and correspond well to modeled changes, and decreases in evapotranspiration in the Northwest, Missouri, and Arkansas are also captured (Fig. 6).

The model and observations also compare well in the absolute daily July–August average value in the two regions (Fig. 6f), especially in the Midwest. This adds confidence to the selection of vegetation parameters that are used to represent the intensification of agricultural productivity. Further exploration of evapotranspiration rates and energy partitioning within various biomes in the model is beyond the scope of this paper but may be explored in a future publication.

5. Decomposition of agricultural development components

To further understand the impact of the three-component agricultural development in this region, shorter sensitivity experiments were conducted where the changes were broken down into the intensification of agriculture and the expansion of both irrigated and nonirrigated cropland. These experiments are conducted with CERA-20C but are performed from 1982 to 2005, and all comparisons are made with simulations run during this period, removing any influence from changing boundary conditions. Unlike the other simulation results shown in this paper, these short-term simulations are composed of a single run, not a three-member ensemble. Setup, land use, and parameters for each of the simulations are described in Table 5.

Intensification of agriculture creates a more cohesive regional impact with a decrease in temperature and an increase in precipitation and evapotranspiration (Figs. 7a,c,e). Alternatively, expansion causes a widespread decrease in precipitation and evapotranspiration, and a mixed temperature impact over agricultural areas (Figs. 7b,d,f). The decreases seen are not surprising, as Sterling et al. (2012) showed that agricultural areas have a higher evapotranspiration rate than grasslands when irrigated and a lower evapotranspiration rate otherwise. Expansion can also be framed here as redistribution of agriculture into the area of interest, as cropland is eliminated east of the Appalachians and develops in the west. The competing effects of land-use change shown here support an argument for careful inclusion of all components of land-use change.

6. Discussion and conclusions

Although there has been past work looking at the climate impact of vegetation changes in the Midwest

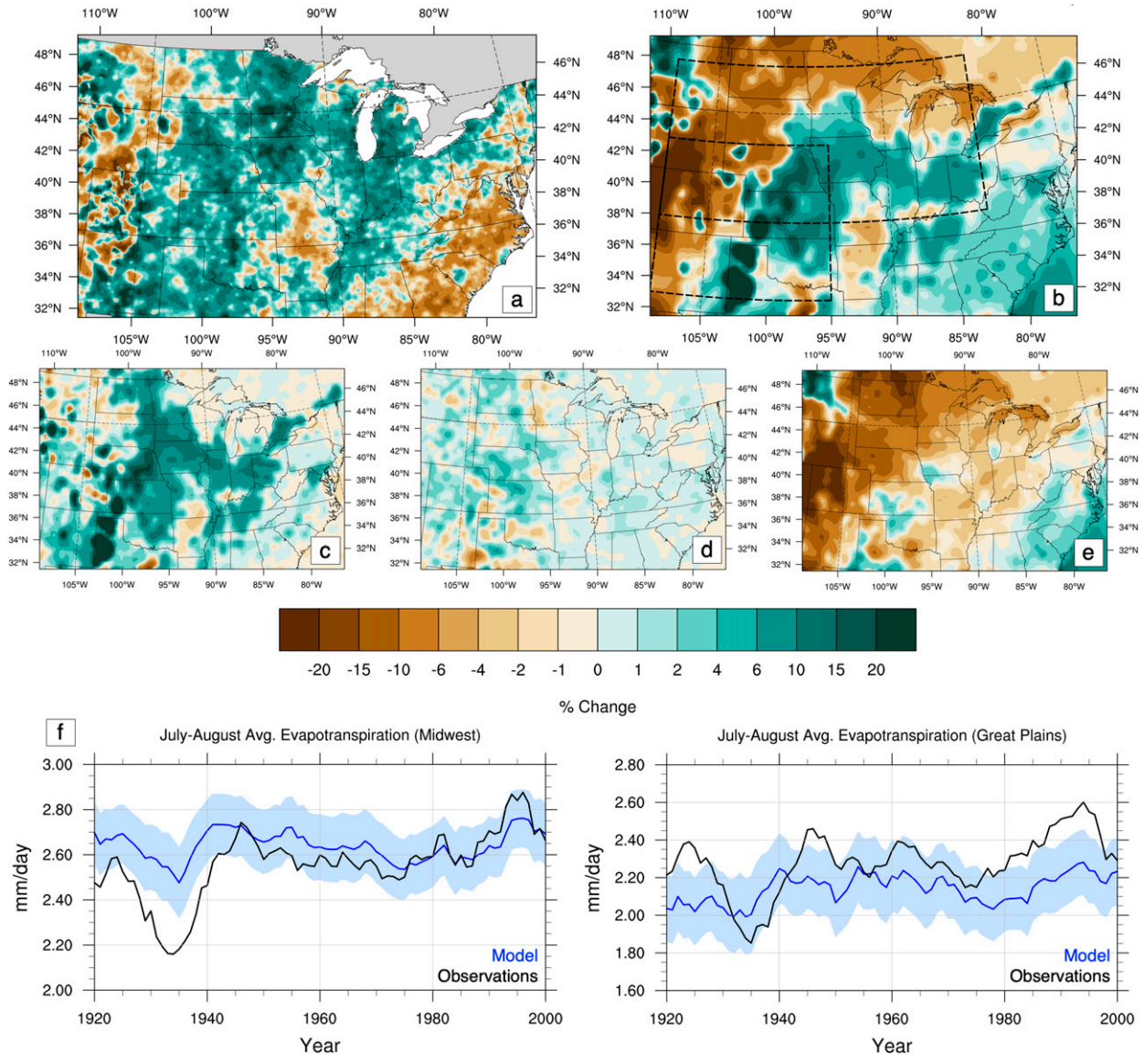

Fig. 6. (a) July–August mean evapotranspiration change from 1920–49 to 1970–99 in VIC data (Livneh et al. 2013), (b) change in V-G simulation, (c) change due to vegetation in simulations, (d) change due to GHG in simulations, and (e) ''residual'' change in simulations due to natural variability, boundary condition errors, and other non-explicitly defined forcings. (f) Time series of area-averaged evapotranspiration in the model ensemble (blue) with shading representing the standard deviation of the three-run ensemble. VIC data are shown in black.

region (Twine et al. 2004; Diffenbaugh 2009; Alter et al. 2015a; Mueller et al. 2015; Alter et al. 2018) this study introduces several important improvements, namely the consideration of continuous expansion and intensification of agriculture throughout the twentieth century, rather than a simple sensitivity study within a single time period. Additionally, only a few studies have focused on a combination of expansion, intensification, and irrigation of cropland in their evolution of land-use and land-cover change in the Midwest. This study utilizes a detailed land-use model as well as recent long-term datasets that allow the evolution of all aspects of agricultural land use change to be represented.

Through careful inclusion of all major components of agricultural development that influence energy and water budget partitioning, this study was able to model the influence of these land-use changes on the regional climate of the Midwest and Great Plains during the twentieth century. Vegetation changes had a substantial impact on temperature in the region, with strong cooling in agreement with observed change, especially given the relatively weak historical GHG effect. Precipitation

TABLE 5. Description of agricultural component experiments. The Pre-Development (PD) experiment is performed with contemporary land-use distribution but pre-intensification productivity. The Full-Development (FD) experiment is performed with contemporary land-use distribution and productivity levels. Pre-Development Plus (PDplus) is performed with early-century land-use distribution and productivity levels.

	Boundary conditions	GHG	Land-use map	Intensification
PD	1982–2005 (CERA-20C)	Evolving (annually)	2000	No
FD	1982–2005 (CERA-20C)	Evolving (annually)	2000	Yes
PDplus	1982–2005 (CERA-20C)	Evolving (annually)	1900	No

variability and change during the period are more complex, and influences from vegetation and GHG are not enough to explain observed precipitation changes. In particular for precipitation, both agricultural intensification and expansion play distinct and occasionally opposing effects on shaping the pattern of changes in this region. The coherent cooling and wetting effect of intensification is modified by shifting land use patterns and the drying that accompanies them. These compounding effects show the importance of carefully considering and including all relevant details of land use forcings.

It is important to consider the areal extent of agriculture and its productivity separately within the climate system for two reasons. First, as shown in the sensitivity studies, they have, at times, opposing effects and modify the energy and water budgets to different degrees. Second, in the course of the twentieth century, and likely in the future, these changes have had different development arcs. While expansion and redistribution of cropland areas was dominant in the early part of the century and continued more modestly in later decades, intensification began in the 1930s and 1940s in the United States and has seen a consistent rise. Future population growth and food demand increase pressure to maintain and improve productivity even while cropland area itself is shrinking (USGCRP 2018; Ray et al. 2012). As the balance of land-use components changes in the future, so will their effects on regional climate. Areas that have seen significant agricultural development in the twentieth century may stabilize in the twenty-first, allowing GHG and other anthropogenic factors to drive future changes in a way that breaks from historical trends. Therefore, it is important to carefully consider each component as well as a holistic view to

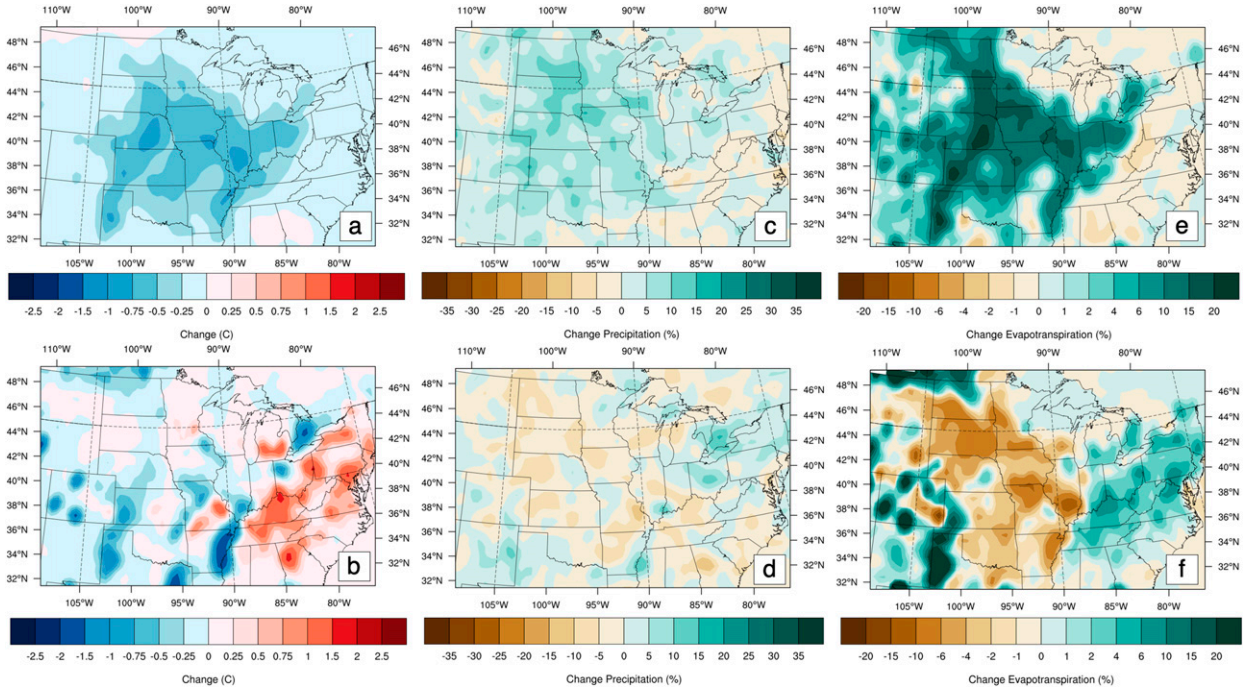

FIG. 7. July–August average temperature changes (°C) in the MRCM short-term simulations (1982–2005) due to (a) intensification of agricultural land only and (b) the expansion of irrigated and nonirrigated cropland with consistent productivity. (c),(d) As in (a),(b), but for precipitation (%). (e),(f) As in (a),(b), but for evapotranspiration (%). Data are plotted using a 9-point smoothing function.

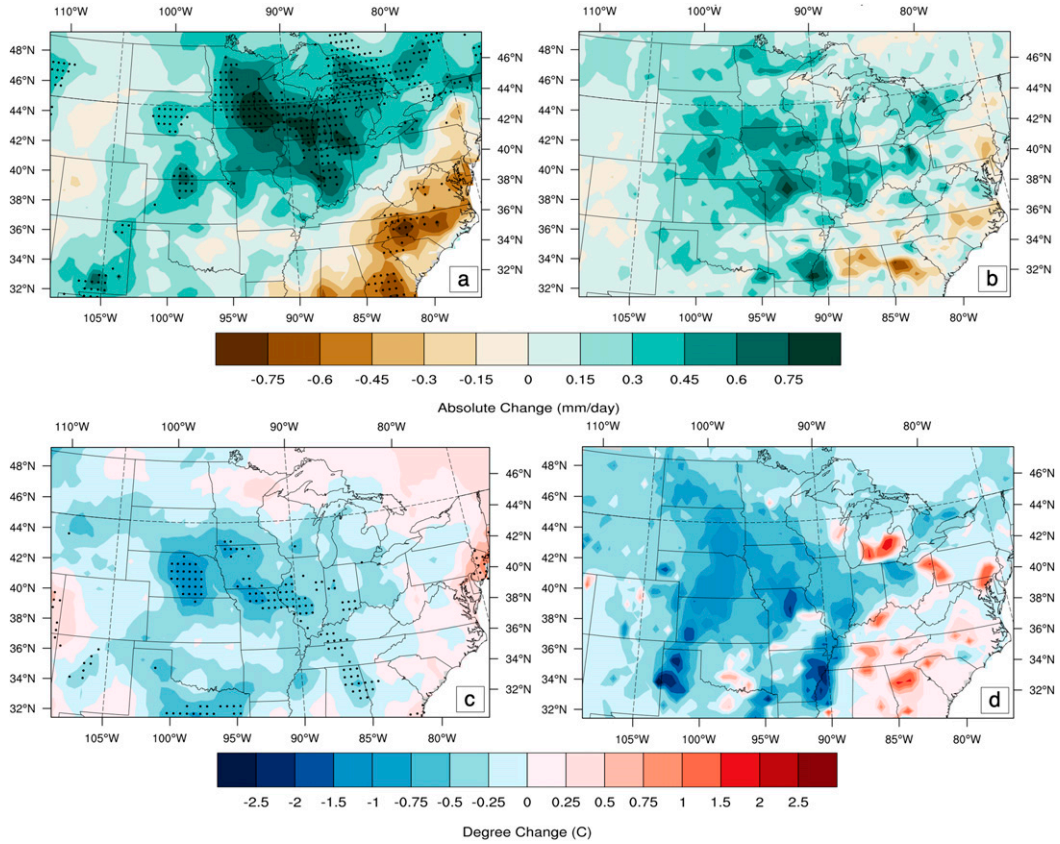

FIG. 8. (a) Observed July–August precipitation change (mm day^{-1}) from 1920–49 to 1970–99 in CRU data. (b) Composite precipitation change in the same period from simulated vegetation and GHG impacts as well as estimated SST influence (individual components shown in Figs. 5c–e). (c) Observed July–August temperature change (°C) from 1920–49 to 1970–99 in CRU data. (d) Composite temperature change in the same period from simulated vegetation and GHG impacts as well as estimated SST influence (individual components shown in Figs. 4c–e).

understand the breakdown of effects as well as realistically depict changes in model simulations. Future work in this area is also an opportunity to further explore the balance between agricultural land use development and reforestation, a breakdown of biome level evapotranspiration changes, and a more granular representation of C_3 versus C_4 crop pathways. Current limitations in this area of study also include the coarse grid-scale representation of areas of irrigated and nonirrigated agricultural as necessitated by the land surface scheme and available data. Further improvements in experiment design would aim to represent the extent of these areas with a higher degree of detail and continue to incorporate new sources of data.

Although the results here show that land-use change has shaped the regional climate changes in this region over the last century, natural internal variability is shown to be influential. Literature has highlighted the strong impact of natural variability in North America (Deser et al. 2012) and in the occurrence of the warming hole itself (Banerjee et al. 2017). An understanding of the importance of these natural variations has been taken into consideration in the multiple member design of this study, and the consideration of nonanthropogenic forcings on the observed changes. The decadal variability of SST patterns, particularly in the Atlantic, seems to have played a role in precipitation changes, with supporting influences from the tropical Pacific and the central North Pacific. The mechanism for this change is probably the strengthening and westward expansion of the North Atlantic subtropical high (NASH) (Wang et al. 2010; Hu et al. 2011).

By combining the three major forcings considered here—agricultural development, GHG, and SST patterns—a superposition of simulation results and observation-based estimates is able to reproduce, to a large degree, the pattern of precipitation and temperature changes that occurred in the central United States during the twentieth century (Fig. 8). The magnitude of temperature changes are overestimated with these three forcings alone, while

precipitation changes are underestimated, but both are able to reproduce the observed spatial pattern of change between the early decades (1920–49) and late decades (1970–99) of the twentieth century.

Future work will focus on the influence of SST patterns in this region and how certain combinations of SST patterns influence periods of increased or decreased precipitation and temperature. This is an important factor to consider in the prediction of long-term drought episodes under future climate scenarios. The climate change caused by this historic agricultural development offers valuable insight for future predictions, as future changes in GHG concentrations, agricultural area, and productivity will modify the balance between forcings. Expanded studies including a more detailed incorporation of aerosol forcing would help to even further characterize the warming hole phenomenon. Competing effects and previously nonincorporated forcings will influence future climate and the occurrence of extreme events such as droughts and heat waves that will affect both population centers and industry in these regions.

Acknowledgments. Thank you to Ross E. Alter and Suchul Kang for modeling and analysis advice, and to Suchul Kang and Alexandre Tuel for providing advice and observations on the results as well as comments on the manuscript. Thank you to Karl Hennerman at ECMWF for instructions and assistance in downloading CERA-20C data. The 20th Century Reanalysis V2c data were provided by the NOAA/OAR/ESRL PSD, Boulder, Colorado, USA, from their web site at https://www.esrl.noaa.gov/psd/. CRU TS3.10 data were retrieved from https://crudata.uea.ac.uk/cru/data/hrg/. Met Office Hadley Centre observation data were retrieved from https://www.metoffice.gov.uk/hadobs/hadisst/data/download.html. This study was supported by funding from the Ida M. Green Fellowship, the Exponent Fellowship, and a seed grant from the Massachusetts Institute of Technology Environmental Solutions Initiative.

REFERENCES

Adegoke, J. O., R. A. Pielke Sr., J. Eastman, R. Mahmood, and K. G. Hubbard, 2003: Impact of irrigation on midsummer surface fluxes and temperature under dry synoptic conditions: A regional atmospheric model study of the U.S. High Plains. *Mon. Wea. Rev.*, **131**, 556–564, https://doi.org/10.1175/1520-0493(2003)131<0556:IOIOMS>2.0.CO;2.

Alfaro, E. J., A. Gershunov, and D. Cayan, 2006: Prediction of summer maximum and minimum temperature over the central and western United States: The roles of soil moisture and sea surface temperature. *J. Climate*, **19**, 1407–1421, https://doi.org/10.1175/JCLI3665.1.

Alter, R. E., Y. Fan, B. R. Lintner, and C. P. Weaver, 2015a: Observational evidence that Great Plains irrigation has enhanced summer precipitation intensity and totals in the Midwestern United States. *J. Hydrometeor.*, **16**, 1717–1735, https://doi.org/10.1175/JHM-D-14-0115.1.

——, E.-S. Im, and E. A. B. Eltahir, 2015b: Rainfall consistently enhanced around the Gezira Scheme in East Africa due to irrigation. *Nat. Geosci. Lett.*, **8**, 763–767, https://doi.org/10.1038/ngeo2514.

——, H. C. Douglas, J. M. Winter, and E. A. Eltahir, 2018: Twentieth century regional climate change during the summer in the central United States attributed to agricultural intensification. *Geophys. Res. Lett.*, **45**, 1586–1594, https://doi.org/10.1002/2017GL075604.

Arakawa, A., and W. H. Schubert, 1974: Interaction of a cumulus cloud ensemble with the large-scale environment, Part I. *J. Atmos. Sci.*, **31**, 674–701, https://doi.org/10.1175/1520-0469(1974)031<0674:IOACCE>2.0.CO;2.

Bandaru, V., T. O. West, D. M. Ricciuto, and R. C. Izaurralde, 2013: Estimating crop net primary production using national inventory data and MODIS-derived parameters. *ISPRS J. Photogramm. Remote Sens.*, **80**, 61–71, https://doi.org/10.1016/j.isprsjprs.2013.03.005.

Banerjee, A., L. M. Polvani, and J. C. Fyfe, 2017: The United States "warming hole": Quantifying the forced aerosol response given large internal variability. *Geophys. Res. Lett.*, **44**, 1928–1937, https://doi.org/10.1002/2016GL071567.

Ben-Ari, T., and D. Makowski, 2014: Decomposing global crop yield variability. *Environ. Res. Lett.*, **9**, 114011, https://doi.org/10.1088/1748-9326/9/11/114011.

Bonfils, C., and D. Lobell, 2007: Empirical evidence for a recent slowdown in irrigation-induced cooling. *Proc. Natl. Acad. Sci. USA*, **104**, 13 582–13 587, https://doi.org/10.1073/pnas.0700144104.

Brown, P. J., and A. T. DeGaetano, 2013: Trends in U.S. surface humidity, 1930–2010. *J. Appl. Meteor. Climatol.*, **52**, 147–163, https://doi.org/10.1175/JAMC-D-12-035.1.

Burgman, R. J., and Y. Jang, 2015: Simulated U.S. drought response to interannual and decadal Pacific SST variability. *J. Climate*, **28**, 4688–4705, https://doi.org/10.1175/JCLI-D-14-00247.1.

Chini, L., G. Hurtt, and S. Frolking, 2014: Harmonized global land use for years 1500–2100, v1. Oak Ridge National Laboratory Distributed Active Archive Center, accessed 23 April 2017, https://doi.org/10.3334/ORNLDAAC/1248.

Compo, G. P., and Coauthors, 2011: The Twentieth Century Reanalysis Project. *Quart. J. Roy. Meteor. Soc.*, **137**, 1–28, https://doi.org/10.1002/qj.776.

Cook, B. I., R. Seager, and R. L. Miller, 2011: Atmospheric circulation anomalies during two persistent North American droughts: 1932–1939 and 1948–1957. *Climate Dyn.*, **36**, 2339–2355, https://doi.org/10.1007/s00382-010-0807-1.

——, T. R. Ault, and J. E. Smerdon, 2015: Unprecedented 21st century drought risk in the American Southwest and Central Plains. *Sci. Adv.*, **1**, e1400082, https://doi.org/10.1126/sciadv.1400082.

DeAngelis, A., F. Dominguez, Y. Fan, A. Robock, M. D. Kustu, and D. Robinson, 2010: Evidence of enhanced precipitation due to irrigation over the Great Plains of the United States. *J. Geophys. Res.*, **115**, D15115, https://doi.org/10.1029/2010JD013892.

Deser, C., R. Knutti, S. Solomon, and A. S. Phillips, 2012: Communication of the role of natural variability in future North American climate. *Nat. Climate Change*, **2**, 775–779, https://doi.org/10.1038/nclimate1562.

Diffenbaugh, N. S., 2009: Influence of modern land cover on the climate of the United States. *Climate Dyn.*, **33**, 945–958, https://doi.org/10.1007/s00382-009-0566-z.

——, J. S. Pal, R. J. Trapp, and F. Giorgi, 2005: Fine-scale processes regulate the response of extreme events to global climate change. *Proc. Natl. Acad. Sci. USA*, **102**, 15 774–15 778, https://doi.org/10.1073/pnas.0506042102.

Donat, M. G., A. D. King, J. T. Overpeck, L. V. Alexander, I. Durre, and D. J. Karoly, 2016: Extraordinary heat during the 1930s US Dust Bowl and associated large-scale conditions. *Climate Dyn.*, **46**, 413–426, https://doi.org/10.1007/s00382-015-2590-5.

Douglas, H., 2016: Observational analysis of twentieth century summer climate over North America. Master's thesis, Department of Civil and Environmental Engineering, Massachusetts Institute of Technology, 96 pp., http://hdl.handle.net/1721.1/104191.

ECMWF, 2017: Reanalysis Datasets: CERA-20C. ECMWF, accessed 31 October 2017, https://www.ecmwf.int/en/forecasts/datasets/reanalysis-datasets/cera-20c.

Eltahir, E. A. B., 1998: A soil moisture–rainfall feedback mechanism: 1. Theory and observations. *Water Resour. Res.*, **34**, 765–776, https://doi.org/10.1029/97WR03499.

Enfield, D. B., A. M. Mestas-Nuñez, and P. J. Trimble, 2001: The Atlantic Multidecadal Oscillation and its relation to rainfall and river flows in the continental U.S. *Geophys. Res. Lett.*, **28**, 2077–2080, https://doi.org/10.1029/2000GL012745.

Findell, K. L., and T. L. Delworth, 2010: Impact of common sea surface temperature anomalies on global drought and pluvial frequency. *J. Climate*, **23**, 485–503, https://doi.org/10.1175/2009JCLI3153.1.

Gianotti, R. L., and E. A. B. Eltahir, 2014a: Regional climate modeling over the Maritime Continent. Part I: New parameterization for convective cloud fraction. *J. Climate*, **27**, 1488–1503, https://doi.org/10.1175/JCLI-D-13-00127.1.

——, and ——, 2014b: Regional climate modeling over the Maritime Continent. Part II: New parameterization for autoconversion of convective rainfall. *J. Climate*, **27**, 1504–1523, https://doi.org/10.1175/JCLI-D-13-00171.1.

——, D. Zhang, and E. A. B. Eltahir, 2012: Assessment of the Regional Climate Model version 3 over the Maritime Continent using different cumulus parameterization and land surface schemes. *J. Climate*, **25**, 638–656, https://doi.org/10.1175/JCLI-D-11-00025.1.

Grell, G. A., 1993: Prognostic evaluation of assumptions used by cumulus parameterizations. *Mon. Wea. Rev.*, **121**, 764–787, https://doi.org/10.1175/1520-0493(1993)121<0764:PEOAUB>2.0.CO;2.

Halder, S., S. K. Saha, P. A. Dirmeyer, T. N. Chase, and B. N. Goswami, 2016: Investigating the impact of land-use land-cover change on Indian summer monsoon daily rainfall and temperature during 1951–2005 using a regional climate model. *Hydrol. Earth Syst. Sci.*, **20**, 1765–1784, https://doi.org/10.5194/hess-20-1765-2016.

Harding, K. J., and P. K. Snyder, 2012: Modeling the atmospheric response to irrigation in the Great Plains. Part I: General impacts on precipitation and the energy budget. *J. Hydrometeor.*, **13**, 1667–1686, https://doi.org/10.1175/JHM-D-11-098.1.

Harris, I., P. D. Jones, T. J. Osborn, and D. H. Lister, 2014: Updated high-resolution grids of monthly climatic observations—The CRU TS3.10 dataset. *Int. J. Climatol.*, **34**, 623–642, https://doi.org/10.1002/joc.3711.

Heckert, N., and J. J. Filliben, 2003: NIST handbook 148: DATAPLOT reference manual, Volume I: Commands. Tech. Rep., National Institute of Standards and Technology Handbook Series, June 2003, https://www.itl.nist.gov/div898/software/dataplot/refman1/homepage.htm.

Hicke, J. A., and D. B. Lobell, 2004: Spatiotemporal patterns of cropland area and net primary production in the central United States estimated from USDA agricultural information. *Geophys. Res. Lett.*, **31**, L20502, https://doi.org/10.1029/2004GL020927.

Hu, Q., S. Feng, and R. J. Oglesby, 2011: Variations in North American summer precipitation driven by the Atlantic multidecadal oscillation. *J. Climate*, **24**, 5555–5570, https://doi.org/10.1175/2011JCLI4060.1.

Huang, B., and Coauthors, 2017: Extended reconstructed sea surface temperature, version 5 (ERSSTv5): Upgrades, validations, and intercomparisons. *J. Climate*, **30**, 8179–8205, https://doi.org/10.1175/JCLI-D-16-0836.1.

Huber, D. B., D. B. Mechem, and N. A. Brunsell, 2014: The effects of Great Plains irrigation on the surface energy balance, regional circulation, and precipitation. *Climate*, **2**, 103–128, https://doi.org/10.3390/cli2020103.

Hurtt, G. C., and Coauthors, 2011: Harmonization of land-use scenarios for the period 1500–2100: 600 years of global gridded annual land-use transitions, wood harvest, and resulting secondary lands. *Climatic Change*, **109**, 117–161, https://doi.org/10.1007/s10584-011-0153-2.

Im, E.-S., and E. A. B. Eltahir, 2014: Enhancement of rainfall and runoff upstream from irrigation location in a climate model of West Africa. *Water Resour. Res.*, **50**, 8651–8674, https://doi.org/10.1002/2014WR015592.

——, M. P. Marcella, and E. A. B. Eltahir, 2014: Impact of potential large-scale irrigation on the West African monsoon and its dependence on location of irrigated area. *J. Climate*, **27**, 994–1009, https://doi.org/10.1175/JCLI-D-13-00290.1.

Jaafar, H. H., and F. A. Ahmad, 2015: Crop yield prediction from remotely sensed vegetation indices and primary productivity in arid and semi-arid lands. *Int. J. Remote Sens.*, **36**, 4570–4589, https://doi.org/10.1080/01431161.2015.1084434.

Jia, L., and Coauthors, 2016: The roles of radiative forcing, sea surface temperatures, and atmospheric and land initial conditions in U.S. summer warming episodes. *J. Climate*, **29**, 4121–4135, https://doi.org/10.1175/JCLI-D-15-0471.1.

Jin, J., and N. L. Miller, 2011: Regional simulations to quantify land use change and irrigation impacts on hydroclimate in the California Central Valley. *Theor. Appl. Climatol.*, **104**, 429–442, https://doi.org/10.1007/s00704-010-0352-1.

Knight, J. R., C. K. Folland, and A. A. Scaife, 2006: Climate impacts of the Atlantic multidecadal oscillation. *Geophys. Res. Lett.*, **33**, L17706, https://doi.org/10.1029/2006GL026242.

Koster, R. D., H. Wang, S. D. Schubert, M. J. Suarez, and S. Mahanama, 2009: Drought-induced warming in the continental United States under different SST regimes. *J. Climate*, **22**, 5385–5400, https://doi.org/10.1175/2009JCLI3075.1.

Kueppers, L. M., M. A. Snyder, and L. C. Sloan, 2007: Irrigation cooling effect: Regional climate forcing by land-use change. *Geophys. Res. Lett.*, **34**, L03703, https://doi.org/10.1029/2006GL028679.

Kunkel, K. E., X.-Z. Liang, J. Zhu, and Y. Lin, 2006: Can CGCMs simulate the twentieth-century "warming hole" in the central United States? *J. Climate*, **19**, 4137–4153, https://doi.org/10.1175/JCLI3848.1.

Laloyaux, P., 2017: The Climate Data Guide: CERA-20C: ECMWF's Coupled Ocean-Atmosphere Reanalysis of the 20th Century. Accessed 31 October 2017, https://climatedataguide.ucar.edu/

climate-data/cera-20c-ecmwfs-coupled-ocean-atmosphere-reanalysis-20th-century.

Li, Z., S. Liu, Z. Tan, N. B. Bliss, C. J. Young, T. O. West, and S. M. Ogle, 2014: Comparing cropland net primary production estimates from inventory, a satellite-based model, and a process-based model in the Midwest of the United States. *Ecol. Modell.*, **277**, 1–12, https://doi.org/10.1016/j.ecolmodel.2014.01.012.

Livneh, B., E. A. Rosenberg, C. Lin, B. Nijssen, V. Mishra, K. M. Andreadis, E. P. Maurer, and D. P. Lettenmaier, 2013: A long-term hydrologically based dataset of land surface fluxes and states for the conterminous United States: Update and extensions. *J. Climate*, **26**, 9384–9392, https://doi.org/10.1175/JCLI-D-12-00508.1.

Lo, M.-H., and J. S. Famiglietti, 2013: Irrigation in California's Central Valley strengthens the southwestern U.S. water cycle. *Geophys. Res. Lett.*, **40**, 301–306, https://doi.org/10.1002/grl.50108.

Lobell, D. B., C. J. Bonfils, L. M. Kueppers, and M. A. Snyder, 2008: Irrigation cooling effect on temperature and heat index extremes. *Geophys. Res. Lett.*, **35**, L09705, https://doi.org/10.1029/2008GL034145.

——, G. Bala, A. Mirin, T. Phillips, R. Maxwell, and D. Rotman, 2009: Regional differences in the influence of irrigation on climate. *J. Climate*, **22**, 2248–2255, https://doi.org/10.1175/2008JCLI2703.1.

Lu, Y., K. Harding, and L. Kueppers, 2017: Irrigation effects on land–atmosphere coupling strength in the United States. *J. Climate*, **30**, 3671–3685, https://doi.org/10.1175/JCLI-D-15-0706.1.

Marcella, M. P., 2013: Biosphere–atmosphere interactions over semi-arid regions: Modeling the role of mineral aerosols and irrigation in the regional climate system. Ph.D. dissertation, Massachusetts Institute of Technology, 282 pp., http://hdl.handle.net/1721.1/79490.

——, and E. A. B. Eltahir, 2010: Effects of mineral aerosols on the summertime climate of southwest Asia: Incorporating subgrid variability in a dust emission scheme. *J. Geophys. Res.*, **115**, D18203, https://doi.org/10.1029/2010JD014036.

——, and ——, 2012: Modeling the summertime climate of Southwest Asia: The role of land surface processes in shaping the climate of semiarid regions. *J. Climate*, **25**, 704–719, https://doi.org/10.1175/2011JCLI4080.1.

Mascioli, N. R., M. Previdi, A. M. Fiore, and M. Ting, 2017: Timing and seasonality of the United States 'warming hole'. *Environ. Res. Lett.*, **12**, 034008, https://doi.org/10.1088/1748-9326/aa5ef4.

Mei, R., and G. Wang, 2011: Impact of sea surface temperature and soil moisture on summer precipitation in the United States based on observational data. *J. Hydrometeor.*, **12**, 1086–1099, https://doi.org/10.1175/2011JHM1312.1.

Meinshausen, M., and Coauthors, 2011: The RCP greenhouse gas concentrations and their extensions from 1765 to 2300. *Climatic Change*, **109**, 213–241, https://doi.org/10.1007/s10584-011-0156-z. (Data sources, acknowledgments, and further information are available online at http://www.pik-potsdam.de/~mmalte/rcps.)

Monfreda, C., N. Ramankutty, and J. A. Foley, 2008: Farming the planet: 2. Geographic distribution of crop areas, yields, physiological types, and net primary production in the year 2000. *Global Biogeochem. Cycles*, **22**, GB1022, https://doi.org/10.1029/2007GB002947.

Mueller, N. D., E. E. Butler, K. A. McKinnon, A. Rhines, M. Tingley, N. M. Holbrook, and P. Huybers, 2015: Cooling of US Midwest summer temperature extremes from cropland intensification. *Nat. Climate Change*, **6**, 317–322, https://doi.org/10.1038/nclimate2825.

Nigam, S., B. Guan, and A. Ruiz-Barradas, 2011: Key role of the Atlantic Multidecadal Oscillation in 20th century drought and wet periods over the Great Plains. *Geophys. Res. Lett.*, **38**, L16713, https://doi.org/10.1029/2011GL048650.

Ozdogan, M., M. Rodell, H. K. Beaudoing, and D. L. Toll, 2010: Simulating the effects of irrigation over the United States in a land surface model based on satellite-derived agricultural data. *J. Hydrometeor.*, **11**, 171–184, https://doi.org/10.1175/2009JHM1116.1.

Pal, J. S., and E. A. B. Eltahir, 2002: Teleconnections of soil moisture and rainfall during the 1993 Midwest summer flood. *Geophys. Res. Lett.*, **29**, 1865, https://doi.org/10.1029/2002GL014815.

Pan, Z., C. Shi, S. Kumar, and Z. Gao, 2017: North Pacific SST forcing on the central United States "warming hole" as simulated in CMIP5 coupled historical and uncoupled AMIP experiments. *Atmos.–Ocean*, **55**, 57–77, https://doi.org/10.1080/07055900.2016.1261690.

Partridge, T. F., J. M. Winter, E. C. Osterberg, D. W. Hyndman, A. D. Kendall, and F. J. Magilligan, 2018: Spatially distinct seasonal patterns and forcings of the U.S. warming hole. *Geophys. Res. Lett.*, **45**, 2055–2063, https://doi.org/10.1002/2017GL076463.

Pielke, R. A., Sr., and Coauthors, 2011: Land use/land cover changes and climate: Modeling analysis and observational evidence. *Wiley Interdiscip. Rev.: Climate Change*, **2**, 828–850, https://doi.org/10.1002/wcc.144.

——, R. Mahmood, and C. McAlpine, 2016: Land's complex role in climate change. *Phys. Today*, **69**, 40–46, https://doi.org/10.1063/PT.3.3364.

Poli, P., and Coauthors, 2016: ERA-20C: An atmospheric reanalysis of the twentieth century. *J. Climate*, **29**, 4083–4097, https://doi.org/10.1175/JCLI-D-15-0556.1.

Prince, S. D., J. Haskett, M. Steininger, H. Strand, and R. Wright, 2001: Net primary production of U.S. Midwest croplands from agricultural harvest yield data. *Ecol. Appl.*, **11**, 1194–1205, https://doi.org/10.1890/1051-0761(2001)011[1194:NPPOUS]2.0.CO;2.

Qian, Y., M. Huang, B. Yang, and L. K. Berg, 2013: A modeling study of irrigation effects on surface fluxes and land–air–cloud interactions in the southern Great Plains. *J. Hydrometeor.*, **14**, 700–721, https://doi.org/10.1175/JHM-D-12-0134.1.

Ramankutty, N., and J. A. Foley, 1999: Estimating historical changes in global land cover: Croplands from 1700 to 1992. *Global Biogeochem. Cycles*, **13**, 997–1027, https://doi.org/10.1029/1999GB900046.

Ray, D. K., N. Ramankutty, N. D. Mueller, P. C. West, and J. A. Foley, 2012: Recent patterns of crop yield growth and stagnation. *Nat. Commun.*, **3**, 1293, https://doi.org/10.1038/ncomms2296.

Rayner, N. A., D. E. Parker, E. B. Horton, C. K. Folland, L. V. Alexander, D. P. Rowell, E. C. Kent, and A. Kaplan, 2003: Global analyses of sea surface temperature, sea ice, and night marine air temperature since the late nineteenth century. *J. Geophys. Res.*, **108**, 4407, https://doi.org/10.1029/2002JD002670.

Roxburgh, S. H., S. L. Berry, T. N. Buckley, B. Barnes, and M. L. Roderick, 2005: What is NPP? Inconsistent accounting of respiratory fluxes in the definition of net primary production. *Funct. Ecol.*, **19**, 378–382, https://doi.org/10.1111/j.1365-2435.2005.00983.x.

Ruiz-Barradas, A., and S. Nigam, 2010: Great Plains precipitation and its SST links in twentieth-century climate simulations, and twenty-first- and twenty-second-century climate projections. *J. Climate*, **23**, 6409–6429, https://doi.org/10.1175/2010JCLI3173.1.

Schubert, S. D., M. J. Suarez, P. J. Pegion, R. D. Koster, and T. Bacmeister, 2004: On the cause of the 1930s Dust Bowl. *Science*, **303**, 1855–1859, https://doi.org/10.1126/science.1095048.

——, and Coauthors, 2009: A U.S. CLIVAR project to assess and compare the responses of global climate models to drought-related SST forcing patterns: Overview and results. *J. Climate*, **22**, 5251–5272, https://doi.org/10.1175/2009JCLI3060.1.

Seager, R., and M. Hoerling, 2014: Atmosphere and ocean origins of North American droughts. *J. Climate*, **27**, 4581–4606, https://doi.org/10.1175/JCLI-D-13-00329.1.

——, Y. Kushnir, M. Ting, M. Cane, N. Naik, and J. Miller, 2008: Would advance knowledge of 1930s SSTs have allowed prediction of the Dust Bowl drought? *J. Climate*, **21**, 3261–3281, https://doi.org/10.1175/2007JCLI2134.1.

Sheskin, D. J., 2007: *Handbook of Parametric and Nonparametric Statistical Procedures*. 4th ed. Taylor & Francis, 1736 pp.

Siebert, S., M. Kummu, M. Porkka, P. Döll, N. Ramankutty, and B. R. Scanlon, 2015: A global data set of the extent of irrigated land from 1900 to 2005. *Hydrol. Earth Syst. Sci.*, **19**, 1521–1545, https://doi.org/10.5194/hess-19-1521-2015.

Simoes, A., 2016a: Observatory of Economic Complexity: Which countries export corn (2016)? Accessed 8 October 2018, http://atlas.media.mit.edu/en/visualize/tree_map/hs92/export/show/all/1005/2016/.

——, 2016b: Observatory of Economic Complexity: Which countries export soybeans (2016)? Accessed 8 October 2018, http://atlas.media.mit.edu/en/visualize/tree_map/hs92/export/show/all/1201/2016/.

Sterling, S. M., A. Ducharne, and J. Polcher, 2012: The impact of global land-cover change on the terrestrial water cycle. *Nat. Climate Change*, **3**, 385–390, https://doi.org/10.1038/nclimate1690.

Ting, M., and H. Wang, 1997: Summertime U.S. precipitation variability and its relation to Pacific sea surface temperature. *J. Climate*, **10**, 1853–1873, https://doi.org/10.1175/1520-0442(1997)010<1853:SUSPVA>2.0.CO;2.

Twine, T. E., C. J. Kucharik, and J. A. Foley, 2004: Effects of land cover change on the energy and water balance of the Mississippi River basin. *J. Hydrometeor.*, **5**, 640–655, https://doi.org/10.1175/1525-7541(2004)005<0640:EOLCCO>2.0.CO;2.

U.S. Census Bureau, 2017: U.S. and World Population Clock. U.S. Census Bureau, https://www.census.gov/popclock/.

USDA-NASS, 2016: Quick Stats. U.S. Department of Agriculture National Agricultural Statistics Service (USDA NASS). Accessed 13 July 2017, https://quickstats.nass.usda.gov/.

USGCRP, 2018: *Impacts, Risks, and Adaptation in the United States*. Vol. II, *Fourth National Climate Assessment*, D. R. Reidmiller et al., Eds., U.S. Global Change Research Program, 1515 pp. https://doi.org/10.7930/NCA4.2018.

Wang, H., and S. Schubert, 2014: The precipitation response over the continental United States to cold tropical Pacific sea surface temperatures. *J. Climate*, **27**, 5036–5055, https://doi.org/10.1175/JCLI-D-13-00453.1.

——, ——, M. Suarez, J. Chen, M. Hoerling, A. Kumar, and P. Pegion, 2009: Attribution of the seasonality and regionality in climate trends over the United States during 1950–2000. *J. Climate*, **22**, 2571–2590, https://doi.org/10.1175/2008JCLI2359.1.

——, ——, ——, and R. Koster, 2010: The physical mechanisms by which the leading patterns of SST variability impact U.S. precipitation. *J. Climate*, **23**, 1815–1836, https://doi.org/10.1175/2009JCLI3188.1.

Weaver, S. J., and S. Nigam, 2008: Variability of the Great Plains low-level jet: Large-scale circulation context and hydroclimate impacts. *J. Climate*, **21**, 1532–1551, https://doi.org/10.1175/2007JCLI1586.1.

——, S. Schubert, and H. Wang, 2009: Warm season variations in the low-level circulation and precipitation over the central United States in observations, AMIP simulations, and idealized SST experiments. *J. Climate*, **22**, 5401–5420, https://doi.org/10.1175/2009JCLI2984.1.

West, T. O., and Coauthors, 2010: Cropland carbon fluxes in the United States: Increasing geospatial resolution of inventory-based carbon accounting. *Ecol. Appl.*, **20**, 1074–1086, https://doi.org/10.1890/08-2352.1.

Winter, J. M., 2006: Coupling of Integrated BIosphere Simulator to Regional Climate Model version 3. Master's thesis, Dept. of Civil and Environmental Engineering, Massachusetts Institute of Technology, 102 pp., http://hdl.handle.net/1721.1/34272.

——, and E. A. B. Eltahir, 2012a: Modeling the hydroclimatology of the Midwestern United States. Part 1: Current climate. *Climate Dyn.*, **38**, 573–593, https://doi.org/10.1007/s00382-011-1182-2.

——, and ——, 2012b: Modeling the hydroclimatology of the Midwestern United States. Part 2: Future climate. *Climate Dyn.*, **38**, 595–611, https://doi.org/10.1007/s00382-011-1183-1.

Zhang, Y., Z. Gao, Z. Pan, D. Li, and B. Wan, 2016: Record-breaking temperatures in China during the warming and recent hiatus periods. *J. Geophys. Res.*, **121**, 241–258, https://doi.org/10.1002/2015JD023886.